Article

Nanochannels of Two Distinct Cross-Sections in a Porous Al-Based Coordination Polymer

Angiolina Comotti, Silvia Bracco, Piero Sozzani, Satoshi Horike, Ryotaro Matsuda, Jinxi Chen, Masaki Takata, Yoshiki Kubota, and Susumu Kitagawa

J. Am. Chem. Soc., **2008**, 130 (41), 13664-13672 • DOI: 10.1021/ja802589u • Publication Date (Web): 18 September 2008

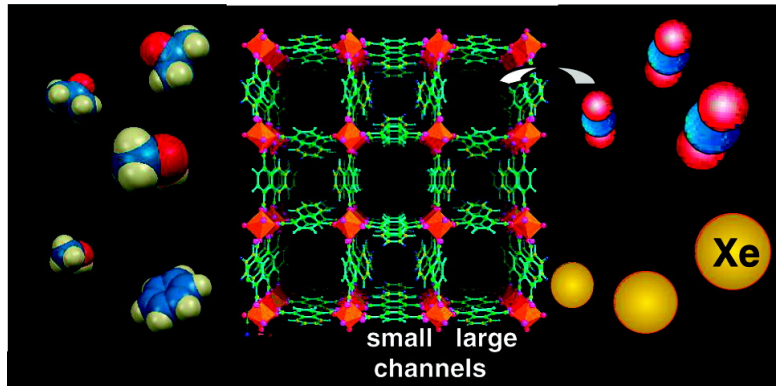

More About This Article

Additional resources and features associated with this article are available within the HTML version:

- Supporting Information
- Access to high resolution figures
- Links to articles and content related to this article
- Copyright permission to reproduce figures and/or text from this article

View the Full Text HTML

J|A|C|S
ARTICLES

Published on Web 09/18/2008

Nanochannels of Two Distinct Cross-Sections in a Porous Al-Based Coordination Polymer

Angiolina Comotti,*,† Silvia Bracco,† Piero Sozzani,† Satoshi Horike,‡ Ryotaro Matsuda,§ Jinxi Chen,‡,|| Masaki Takata,⊥ Yoshiki Kubota,# and Susumu Kitagawa‡

Department of Materials Science, University of Milano-Bicocca and INSTM, Via R. Cozzi 53, 20125 Milan, Italy, Department of Synthetic Chemistry and Biological Chemistry, Graduate School of Engineering, Kyoto University, Katsura, Nishikyo-ku, Kyoto 615-8510, Japan, Structural Materials Science Laboratory, Harima Institute, RIKEN SPring-8 Center and CREST, JST Sayo-gun, Hyogo, 679-5148, Japan, Exploratory Research for Advanced Technology (ERATO), Japan Science and Technology Agency (JST), Kyoto 600-8815, Japan, and Department of Physical Science, Osaka Prefecture University, Sakai, Osaka 599-8531, Japan

Received April 14, 2008; E-mail: angiolina.comotti@mater.unimib.it

Abstract: A new aluminum naphthalenedicarboxylate Al(OH)(1,4-NDC)·$2H_2O$ compound has been synthesized. The crystal structure exhibits a three-dimensional framework composed of infinite chains of corner-sharing octahedral Al(OH)$_2O_4$ with 1,4-naphthanedicarboxylate ligands forming two types of channels with squared-shape cross-section. The large channels present a cross-section of 7.7 × 7.7 Å^2, while the small channels are about 3.0 × 3.0 Å^2. When water molecules are removed, no structural transformation occurs, generating a robust structure with permanent porosity and remarkable thermal stability. 2D $^1H-^{13}C$ heteronuclear correlation NMR measurements, together with the application of Lee-Goldburg homonuclear decoupling, were applied, for the first time, to porous coordination polymers revealing the spatial relationships between the ^1H and ^{13}C spin-active nuclei of the framework. To demonstrate the open pore structure and the easy accessibility of the nanochannels to the gas phase, highly sensitive hyperpolarized (HP) xenon NMR, under extreme xenon dilution, has been applied. Xenon can diffuse selectively into the large nanochannels, while the small ones show no substantial uptake of xenon due to severe restrictions along the channels that prevent the diffusion. Two-dimensional exchange experiments showed the exchange time to be as short as 15 ms. Through variable-temperature HP ^{129}Xe NMR experiments we were able to achieve an unprecedented description of the large nanochannel space and surface, a physisorption energy of 10 kJ mol^{-1}, and the chemical shift value of xenon probing the internal surfaces. The large pore channels are straight, parallel, and independent, allowing one-dimensional anisotropic diffusion of gases and vapors. Their walls are composed of the naphthalene moieties that create an unique environment for selective sorption. These results prompted us to measure the storage capacity toward methanol, acetone, benzene, and carbon dioxide. The selective adsorption of methanol and acetone vs that of water, together with the permanent porosity and high thermal stability, makes this compound a suitable matrix for separation and purification.

Introduction

Recent years have seen the evolution of a new class of porous materials known collectively as metal−organic framework materials (MOFs) or porous coordination polymers (PCPs).[1] They present diverse open architectures and adsorptive functions having potential applications in many fields including separation, purification, entrapping of pharmaceuticals and gas storage.[2] Their great diversity and the modularity of the organic moieties make them competitive with zeolites in adsorption and many potential applications in catalysis can be envisaged.[3] These attractive functions have been based on crystal structure, and in recent years, not only crystallographic studies but dynamic aspects of framework and adsorption properties have been highlighted because several compounds represent unique guest-responsive framework.[4] The storage of important gases and vapors, such as methane, hydrogen, acetylene, ethanol, carbon dioxide, and benzene, has been achieved, enforcing the application of these frameworks in the field of energy and environment.[5]

† Department of Materials Science, University of Milano-Bicocca.
‡ Department of Synthetic Chemistry and Biological Chemistry, Kyoto University.
§ Japan Science and Technology Agency (JST).
|| Current address: School of Chemistry & Chemical Engineering, Southeast University, Nanjing 211189, Jiangsu, P. R. China.
⊥ Structural Materials Science Laboratory, Harima Institute.
Osaka Prefecture University.

(1) (a) Bradshaw, D.; Claridge, J. B.; Cussen, E. J.; Prior, T. J.; Rosseinsky, M. J. *Acc. Chem. Res.* **2005**, *38*, 273–282. (b) Férey, G.; Mellot-Draznieks, C.; Serre, C.; Millange, F. *Acc. Chem. Res.* **2005**, *38*, 217–225. (c) Kitagawa, S.; Kitaura, R.; Noro, S. *Angew. Chem., Int. Ed.* **2004**, *43*, 2334–2375. (d) Yaghi, O. M.; O'Keeffe, M.; Ockwig, N. W.; Chae, H. K.; Eddaudi, M.; Kim, J. *Nature* **2003**, *423*, 705. (e) James, S. L. *Chem. Soc. Rev.* **2003**, *32*, 276–288. (f) Kesanli, B.; Lin, W. B. *Coord. Chem. Rev.* **2003**, *246*, 305–326.

 10.1021/ja802589u CCC: $40.75

To investigate the structure and adsorption properties of the porous metal−organic materials, NMR spectroscopic techniques have been less commonly applied.[6] They can depict not only the interfaces and structure but are also capable of understanding the location of guest species in the cavities and describe the shape and size of the empty spaces accessible to sorbates in porous materials.[7] Therefore, the development of spectroscopic analysis for PCP compounds is regarded as an essential approach for in-depth understanding of the structure, adsorption functions and properties. In other sorbents such as zeolite, organic host, and silica-based mesoporous materials, solid state NMR spectroscopy has been one of the most powerful techniques to characterize the porous structure and sorption mechanism.[8] In particular, multinuclear, two-dimensional (2D) solid-state nuclear magnetic resonance spectroscopy, being sensitive to interatomic distances and dynamics, allows molecular structures to be probed.[9] By the measurement of the heteronuclear dipole−dipole interactions between nuclei, it is possible to determine interactions and distances within the host framework and detect also the spatial relationships of hydrogens, such as hydroxylic groups and water hydrogens, with the neighboring atoms, which are sometimes difficult to be localized by powder X-ray diffraction. In addition, the spectroscopy of spin-active gases diffused to the nanochannels collects information about the shape and size of available cavities. In this respect, Xenon NMR spectroscopy has been a remarkable technique for the study of the nature of micro- and mesoporous materials.[10] The sensitivity of ^{129}Xe NMR can be enhanced by orders of magnitude by laser-assisted hyperpolarized technique (HP) that produces a significant xenon signal even at very low concentrations.[11] By continuous flow technique, hyperpolarized Xe can be continuously delivered to the sample allowing, the recording of 2D exchange spectra and collecting information on the accessibility of the nanochannels. The above-described NMR advanced techniques can work synergistically to give a complete picture of material that possesses dual aspects: the robust and solid framework, and the accessible and empty nanopores.

In this report, the combination of multinuclear solid state NMR, hyperpolarized ^{129}Xe NMR, together with synchrotron X-ray diffraction and adsorption measurements, were used to investigate the structural relationship and adsorption properties of an Al^{3+} microporous coordination polymer with straight 1D channels. We exploited the most advanced solid-state NMR techniques to define the nanostructure and the nanochannel walls, these being of vital importance for the tailoring of new adsorption and separation properties. 2D solid state NMR spectroscopy, including ^{1}H−^{13}C Lee-Goldburg experiments, can reveal the arrangement of the framework.[12] Using the advanced spectroscopy of hyperpolarized ^{129}Xe gas, we were able to address the accessibility and the selectivity of the nanochannels as well as the exchange times with the gas phase, elucidating the behavior of adsorption process between gas phase and PCP interface. Adsorption measurements were able to highlight the storage capacity and selectivity of important gases. These analytical aspects will make clear the nature of PCP framework and sorption properties toward potential applications.

Experimental Section

Synthesis of Al(OH)(1,4-NDC)·2H$_2$O (1). The mixture of $Al(NO_3)_3 \cdot 9H_2O$ (0.375 g, 1.0 mmol), 1,4-H_2NDC (0.108 g, 0.5 mmol), and H_2O (10 mL) was placed in a 23 mL Teflon autoclave and then heated at 180 °C for 1 day. The initial pH value of the reactive solution was 2.5, and the final pH value was 2.0. After filtering off and washing with distilled water, light-yellow powder

(2) (a) Kondo, M.; Yoshitomi, T.; Seki, K.; Matsuzaka, H.; Kitagawa, S. *Angew. Chem., Int. Ed.* **1997**, *36*, 1725–17275. (b) Bourrelly, S.; Llewellyn, P. L.; Serre, C.; Millange, F.; Loiseau, T.; Férey, G. *J. Am. Chem. Soc.* **2005**, *127*, 13519–13521. (c) Chen, B. L.; Ockwig, N. W.; Millward, A. R.; Contreras, D. S.; Yaghi, O. M. *Angew. Chem., Int. Ed.* **2005**, *44*, 4745–4749. (d) Zhao, X. B.; Xiao, B.; Fletcher, A. J.; Thomas, K. M.; Bradshaw, D.; Rosseinsky, M. J. *Science* **2004**, *306*, 1012–1015.

(3) (a) Ohmori, O.; Fujita, M. *Chem. Commun.* **2004**, 1586–1587. (b) Wu, C. D.; Hu, A.; Zhang, L.; Lin, W. B. *J. Am. Chem. Soc.* **2005**, *127*, 8940–8941. (c) Chang, J. S.; Hwang, J. S.; Jhung, S. H.; Park, S. E.; Férey, G.; Cheetham, A. K. *Angew. Chem., Int. Ed.* **2004**, *43*, 2819–2822. (d) Hasegawa, S.; Horike, S.; Matsuda, R.; Furukawa, S.; Mochizuki, K.; Kinoshita, Y.; Kitagawa, S. *J. Am. Chem. Soc.* **2007**, *129*, 2607–2614.

(4) (a) Kitaura, R.; Seki, K.; Akiyama, G.; Kitagawa, S. *Angew. Chem., Int. Ed.* **2003**, *42*, 428–430. (b) Cussen, E. J.; Claridge, J. B.; Rosseinsky, M. J.; Kepert, C. J. *J. Am. Chem. Soc.* **2002**, *124*, 9574–9581. (c) Seki, K. *Phys. Chem. Chem. Phys.* **2002**, *4*, 1968–1971. (d) Serre, C.; Millange, F.; Thouvenot, C.; Nogues, M.; Marsolier, G.; Louer, D.; Ferey, G. *J. Am. Chem. Soc.* **2002**, *124*, 13519–13526.

(5) (a) Rowsell, J. L. C.; Yaghi, O. M. *Angew. Chem., Int. Ed.* **2005**, *44*, 4670–4679. (b) Matsuda, R.; Kitaura, R.; Kitagawa, S.; Kubota, Y.; Belosludov, R. V.; Kobayashi, T. C.; Sakamoto, H.; Chiba, T.; Takata, M.; Kawazoe, Y.; Mita, Y. *Nature* **2005**, *436*, 238–241. (c) Noro, S.; Kitagawa, S.; Kondo, M.; Seki, K. *Angew. Chem., Int. Ed.* **2000**, *39*, 2082–2084.

(6) (a) Uemura, T.; Kitagawa, K.; Horike, S.; Kawamura, T.; Kitagawa, S.; Mizuno, M.; Endo, K. *Chem. Commun.* **2005**, 5968–5970. (b) Horike, S.; Matsuda, R.; Kitaura, R.; Kitagawa, S.; Iijima, T.; Endo, K.; Kubota, Y.; Takata, M. *Chem. Commun.* **2004**, 2152–2153. (c) Loiseau, T.; Serre, C.; Huguenard, C.; Fink, G.; Taulelle, F.; Henry, M.; Bataille, T.; Férey, G. *Chem.−Eur. J.* **2004**, *10*, 1373–1382. (d) Volkringer, C.; Popov, D.; Loiseau, T.; Guillou, N.; Ferey, G.; Haouas, M.; Taulelle, F.; Mellot-Draznieks, C.; Burghammer, M.; Riekel, C. *Nat. Mater.* **2007**, *6*, 760–764. (e) Gonzalez, J.; Devi, R. N.; Tunstall, D. P.; Cox, P. A.; Wright, P. A. *Microporous Mesoporous Mater.* **2005**, *84*, 97–104. (f) Pawsey, S.; Moudrakovski, I.; Ripmeester, J.; Wang, L.-Q.; Exarhos, G. J.; Rowsell, J. L.; Yaghi, O. M. *J. Phys. Chem. C* **2007**, *111*, 6060–6067. (g) Campbell, K.; Ooms, K. J.; Wasylishen, R. E.; Tykwinski, R. R. *Org. Lett.* **2005**, *7*, 3397–3400.

(7) (a) Epping, J. D.; Chmelka, B. F. *Curr. Opin. Colloid Interface Sci.* **2006**, *11*, 81–117. (b) Ripmeester, J. A.; Ratcliffe, C. I. *J. Phys. Chem.* **1990**, *94*, 7652–7656. (c) Jameson, C. *Chem. Rev.* **1991**, *91*, 1375–1395. (d) Comotti, A.; Bracco, S.; Ferretti, L.; Valsesia, P.; Sozzani, P. *J. Am. Chem. Soc.* **2007**, *129*, 8566–8576. (e) Sozzani, P.; Comotti, A.; Bracco, S.; Simonutti, R. *Chem. Commun.* **2004**, 768. (f) Sozzani, P.; Comotti, A.; Bracco, S.; Simonutti, R. *Angew. Chem., Int. Ed.* **2004**, *43*, 2792. (g) Sozzani, P.; Bracco, S.; Comotti, A.; Ferretti, L.; Simonutti, R. *Angew. Chem., Int. Ed.* **2005**, *44*, 1816–1820.

(8) (a) Fyfe, C.; Brouwer, D. H. *J. Am. Chem. Soc.* **2006**, *128*, 11860–11871. (b) Janicke, M. T.; Landry, C. C.; Christiansen, S. C.; Kumar, D.; Stucky, G. D.; Chmelka, B. F. *J. Am. Chem. Soc.* **1998**, *120*, 6940–6951. (c) Baldus, M. *Angew. Chem., Int. Ed.* **2006**, *45*, 1186–1188.

(9) (a) Vega, A. J. *J. Am. Chem. Soc.* **1988**, *110*, 1049–1054. (b) van Rossum, B.-J.; Forster, H.; de Groot, H. J. M. *J. Magn. Reson.* **1997**, *124*, 516–519. (c) Lesage, A.; Charmont, P.; Steuernagel, S.; Emsley, L. *J. Am. Chem. Soc.* **2000**, *122*, 9739. (d) Iuga, D.; Morais, C.; Gan, Z.; Neuville, D. R.; Cormier, L.; Massiot, D. *J. Am. Chem. Soc.* **2005**, *127*, 11540–11541.

(10) (a) Ito, T.; Fraissard, J. *J. Chem. Phys.* **1982**, *76*, 5225–5229. (b) Ripmeester, J. A. *J. Am. Chem. Soc.* **1982**, *104*, 289–290. (c) Moudrakovski, I. L.; Nossov, A.; Lang, S.; Breeze, S. R.; Ratcliffe, C. I.; Simard, B.; Santyr, G.; Ripmeester, J. A. *Chem. Mater.* **2000**, *12*, 1181–1183.

(11) (a) Raftery, D.; Long, H.; Meersmann, T.; Grandinetti, P. J.; Reven, L.; Pines, A. *Phys. Rev. Lett.* **1991**, *66*, 584–587. (b) Haake, M.; Pines, A.; Reimer, J. A.; Seydoux, R. *J. Am. Chem. Soc.* **1997**, *119*, 11711–11712.

(12) (a) Vinogradov, E.; Madhu, P. K.; Vega, S. *Chem. Phys. Lett.* **1999**, *314*, 443–450. (b) Lee, M.; Goldburg, W. I. *Phys. Rev.* **1965**, *140*, 1261–1271. (c) van Rossum, B.-J.; Förster, H.; de Groot, H. J. M. *J. Magn. Reson.* **1997**, *124*, 516–519. (d) Sozzani, P.; Bracco, S.; Comotti, A.; Simonutti, R.; Camurati, I. *J. Am. Chem. Soc.* **2003**, *125*, 2095–2098. (e) Lesage, A.; Sakellariou, D.; Hediger, S.; Elena, B.; Charmont, P.; Steuernagel, S.; Emsley, L. *J. Magn. Reson.* **2003**, *163*, 105–113.

Table 1. Crystallographic Data and Rietveld Refinement Summary for **1** at 300 K

	1
Chemical formula	$C_{12}H_6Al_1O_8$
Formula weight	305.15
Crystal system	Tetragonal
Space group	*P4/nmm* (No. 129)
a (Å)	21.1012 (7)
b (Å)	21.1012 (7)
c (Å)	6.6095 (4)
V (Å^3)	2942.9 (2)
Z	8
Radiation (Å)	0.80070
2θ range	$2.5 < 2\theta < 30.0$
R_{wp}	0.065
R	0.036

of **1** was obtained in pure phase (yield: 80%). The sample was subjected to water evacuation at 150 °C for 12 h and 10^{-3} torr, giving rise to the anhydrous sample **2**.

X-Ray Analysis of Al(OH)(1,4-NDC)·2H$_2$O (1). The structure determination was performed using brilliance synchrotron powder diffraction data which were measured with the large Debye−Scherrer camera and imaging plate as detectors on the BL02B2 beam line at the Super Photon Ring (SPring-8, Hyogo, Japan).[13] The patterns were indexed by using the indexing program TREOR and DICVOL91.[14] A good quality unit cell refinement was obtained by using the structureless Le Bail fitting method.[15] The FOX software, which combines a rigid body and a Monte Carlo approach in the real space, was used to find the initial positions of atoms for Rietveld analysis. The final structure was refined by Rietveld technique. The reliability factors based on the Bragg intensities R_I and the weighted profile *R* factor R_{wp} of the final Rietveld fitting were 3.6 and 6.5%, respectively. The crystal data are reported in Table 1.

Thermogravimetric Analysis. The thermogravimetric trace, performed under N_2 atmosphere at 5 °C min^{-1}, of compound **1** shows two-step weight loss. The first step at about 50 °C is assigned to the removal of water molecules. It accounts for 13% weight loss corresponding to two water molecules per chemical formula (calc: 12.2%). The second step from 250 to 400 °C can be attributed to the departure of OH groups (obs: 6%; calc: 5.8%).

Solid-State NMR. The solid-state NMR spectra were run at 75.5 MHz for ^{13}C on a Bruker Avance 300 instrument operating at a static field of 7.04 T equipped with a 4 mm double resonance MAS probe. The samples were spun at the magic angle at a spinning speed of 15 kHz, and Ramped-Amplitude Cross-Polarization (RAMP-CP) transfer of magnetization was applied. The 90° pulse for proton was 2.9 μs. ^{13}C single-pulse excitation (SPE) experiments were run using a recycle delay of 100 s and cross polarization (CP) MAS experiments were performed using a recycle delay of 10 s and contact times of 2.5 ms. ^{1}H MAS NMR experiments were performed with a recycle delay of 20 s.

Phase-modulated Lee-Goldburg (PMLG) heteronuclear ^{1}H−^{13}C correlation (HETCOR) experiments coupled with fast magic angle spinning (15 kHz) allow the recording of 2D spectra with high resolution both in the hydrogen and carbon dimensions. A few homonuclear decoupling techniques can promote high resolution in the hydrogen domain, such as DUMBO and Lee-Godburg decoupling.[12] Narrow hydrogen resonances, with line widths in the order of 1−2 ppm, could be achieved with Lee-Goldburg homonuclear decoupling during t_1; this resolution permits a sufficiently accurate determination of the proton species present in the system. PMLG ^{1}H−^{13}C HETCOR spectra were run with LG period of 18.9 μs. The efficient transfer of magnetization to the carbon nuclei was performed applying RAMP-CP sequence. Quadrature detection in t_1 was achieved by the time proportional phase increments method. Carbon signals were acquired during t_2 under proton decoupling applying two-pulse phase modulation scheme (TPPM).[16] Before each heteronuclear experiment, samples are outgassed overnight at 160 °C and inserted in the ZrO_2 rotors in a dry box under nitrogen atmosphere.

Hyperpolarized Xe NMR. Hyperpolarization ^{129}Xe NMR experiments were performed by a home-built apparatus with a continuous-flow delivery of hyperpolarized xenon gas with a Bruker Avance 300 spectrometer operating at a Larmor Frequency of 83.02 MHz for ^{129}Xe. A diode array laser delivering 16 W at 795 nm was applied. A stream of gas mixture containing 2% xenon, 2% nitrogen, and 96% helium was used in most of the experiments, and gas flow rates were optimized between 200−300 cm^3/min. The polarization was about 5%. The samples were pressed and outgassed overnight at 150 °C. Then they were inserted in the coil and equilibrated in the gas stream for at least 20 min before collecting the NMR spectra. Typically the spectra were recorded with 128 scans and 0.5 s of recycle delays. A pulse duration of 7 μs was applied. Variable temperatures were achieved by flowing cooled or heated nitrogen gas around the sample region. Two-dimensional (2D) exchange NMR is a powerful technique to investigate dynamic processes occurring on a time-scale up to several seconds.[17] The 2D exchange experiments were run with spectral width of 29 kHz in both t_1 and t_2 dimensions. There were 128 t_1 increments. 2D data were collected in TPPI mode. Mixing times were varied from 1 to 50 ms. The ^{129}Xe NMR chemical shifts were referenced to xenon gas extrapolated to zero pressure.

Gas and Vapor Adsorption Measurements. The adsorption isotherm measurements for nitrogen at 77 K, carbon dioxide at 195 K, and water, ethanol, acetone, and benzene at 298 K were carried out using a volumetric adsorption instrument BELSORP18 from Bel Japan, Inc. A known weight of the compound **1**, typically 200 mg, was placed into a sample tube, then the change of the pressure was monitored and the degree of adsorption was measured by the decrease of the pressure at the equilibrium state.

Results and Discussion

Crystal Structure. The structure of compound **1**, as solved on the basis of synchrotron X-ray diffraction pattern (Figure 1), consists of a three-dimensional framework built up from the connection of infinite chains of corner-sharing octahedral $Al(OH)_2O_4$ with 1,4-naphthanedicarboxylate ligands. The basic structural motif of Al−OH−Al chains along the *c* axis of this compound is identical to the Al^{3+} porous frameworks reported by Férey and Loiseau.[6,18] In our case, the bulky naphthalene rings of organic ligands are projected to the pore surface, resulting in the formation of two kinds of pore apertures with square shapes.

The Al^{3+} is coordinated to four oxygen atoms from four carboxylic groups and two hydroxyl groups located in *trans* position. Bond valence calculations, which generate values of 1.30, confirm the occurrence of a hydroxide anion on the axial oxygen, required for the electroneutrality balance of the structure. The $Al(OH)_2O_4$ units are linked to each other through the two opposite hydroxyl groups and this generates an infinite

(13) Nishibori, E.; Takata, M.; Kato, K.; Sakata, M.; Kubota, Y.; Aoyagi, S.; Kuroiwa, Y.; Yamakata, M.; Ikeda, N. *J. Phys. Chem. Solids* **2001**, *62*, 2095–2098.
(14) Boultif, A.; Louer, D. *J. Appl. Crystallogr.* **1991**, *24*, 987–993.
(15) Lebail, A.; Duroy, H.; Fourquet, J. L. *Mater. Res. Bull.* **1988**, *23*, 447–452.
(16) Bennett, A. E.; Rienstra, C. M.; Auger, M.; Lakshmi, K. V.; Griffin, R. G. *J. Chem. Phys.* **1995**, *103*, 6951–6958.
(17) (a) Zook, A. L.; Adhyaru, B. B.; Bowers, C. R. *J. Magn. Reson.* **2002**, *159*, 175–182. (b) Jeener, J.; Meier, B. H.; Bachmann, P.; Ernst, R. R. *J. Chem. Phys.* **1979**, *71*, 4546–4553.
(18) Loiseau, T.; Mellot-Draznieks, C.; Muguerra, H.; Férey, G.; Haouas, M.; Taulelle, F. C. R. *Chimie* **2005**, *8*, 765–772.

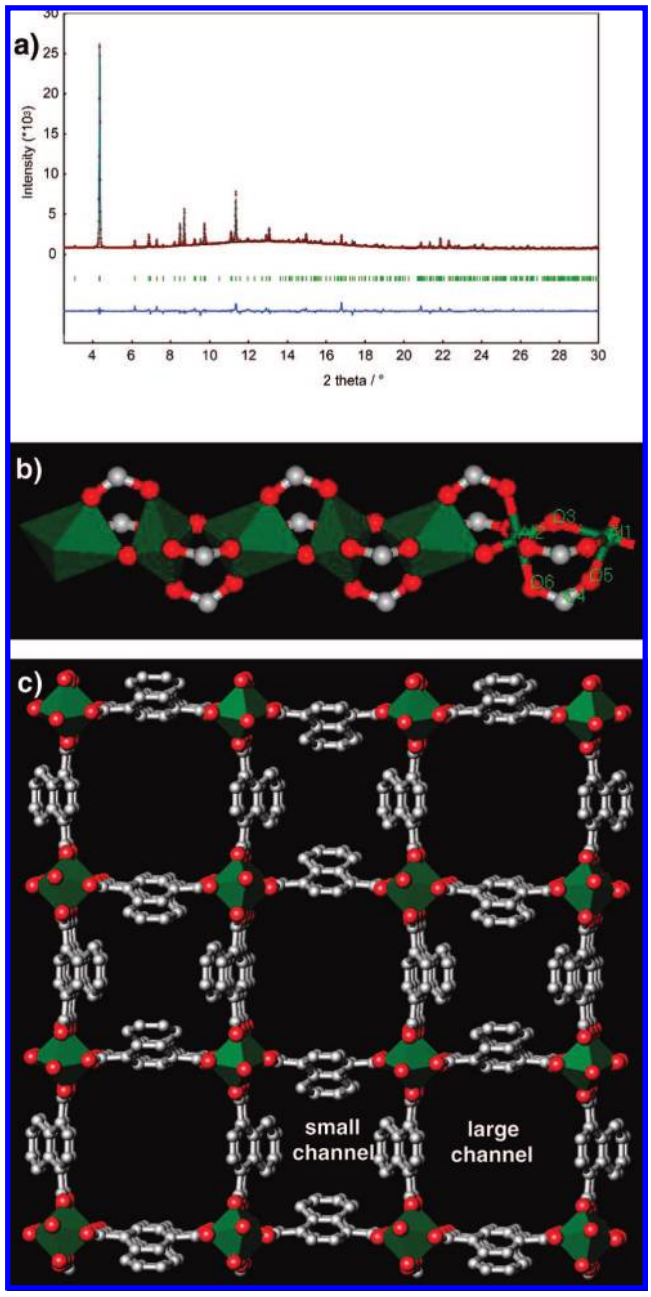

Figure 1. (a) Synchrotron X-ray powder diffraction pattern and the least-squares fitting Rietveld refinement of compound **1**. Comparison of the simulated X-ray pattern predicted for **1** (red) with that of the experimental (black) measured by synchrotron beam. The difference profile is reported in blue. (b) Arrangement of the chain of corner-sharing octahedral $Al(OH)_2O_4$ units. (c) Crystal packing along *c* direction showing two types of square-shaped channels of 7.7 × 7.7 Å^2 and 3 × 3 Å^2 in compound **1**. Oxygen of water molecules and hydrogens of 1,4-NDC are omitted for clarity.

chain running along the *c* axis. The infinite Al−OH−Al chains are interconnected by the 1,4-naphthalenedicarboxylate groups, creating two types of square-shaped channels parallel to the *c* axis. Each channel is delimited by four walls of naphthyl units and four chains of aluminum octahedra. All the C6 and C7 atoms of the naphthyl groups associated with a wall are found on one side. The walls are arranged so that the four walls surrounding a small channel have all the C6 and C7 atoms of the naphthyl groups projecting into that channel. The four walls surrounding the other channels are able to accommodate guest water

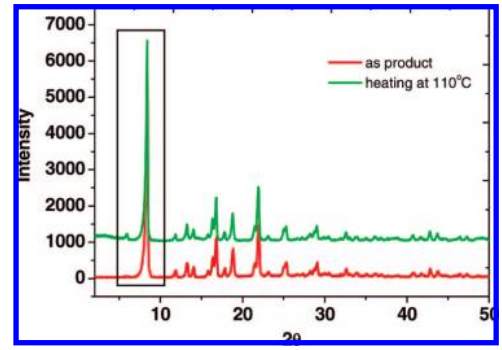

Figure 2. Powder X-ray diffraction patterns of samples **1** (red) and **2** (green).

molecules (2 H_2O molecules per chemical formula) and are called large channels. On the basis of the crystallographic data and the van der Walls radii of atoms, the size of the large channels is about 7.7 × 7.7 Å^2, whereas that of the small channels is about 3.0 × 3.0 Å^2.

Powder X-ray diffraction pattern of sample **2**, freed from water, does not show substantial changes except for the intensity increase of the peaks at 2θ angles lower than 10° because of the increase of the electron density contrast generated by the absence of water molecules within the pores (Figure 2, the powder X-ray diffraction pattern of the compound **1** is reported for comparison). This result suggests that the pore dimension and geometry of sample **2** are similar to that of sample **1** but, in compound **2**, the structure is porous and contains an array of independent and empty channels. The thermogravimetric trace of compound **1** (Supporting Information) indicates the complete removal of two water molecules per chemical formula that is in agreement with stoichiometric water originally present in the large channels of the crystal structure. Interestingly, the Al^{3+} based PCP compound **2** shows the unusual property of a rigid and robust framework where the naphthalene moieties lining the channel walls install $\pi\cdots\pi$ intermolecular interactions (d(C−C) = 3.5−4.6 Å), playing a significant role to promote the robustness of the system. The thermal stability, after removal of water, was checked by thermogravimetric analysis and the guest-free crystalline structure is stable over 300 °C (see Supporting Information).

NMR Characterization. Multinuclear solid state NMR can provide additional information on the structure and topological relationships between spin-active nuclei in the framework. The ^{13}C MAS NMR spectrum of the nanoporous compound reveals well-resolved signals in the downfield region that encompasses the carboxylic and the aromatic carbons. A fully relaxed spectrum, performed with a long recycle delay of 100 s, shows 6 resonances of the same intensity indicating the high symmetry of the framework that allows us to describe the 12 carbons of the building blocks by a minimal unit of 6 independent carbons. A single signal for the carboxylate at 175.2 ppm confirms the occurrence of a constant state of coordination to the metal atoms (Supporting Information ^{13}C MAS and CP MAS NMR spectra). These results support the formation of a highly symmetric framework, the purity of the sample, and a complete absence of an amorphous phase. $^1H-^{13}C$ 2D heterocorrelated spectra, performed with Lee-Goldburg decoupling and high spinning speed, showed high resolution also in the hydrogen domain (Figure 3). The interplay of ^1H and ^{13}C nuclei in the 2D heteronuclear correlation NMR measurements enable the detection of the spatial relationships (<5 Å) between the spin-active

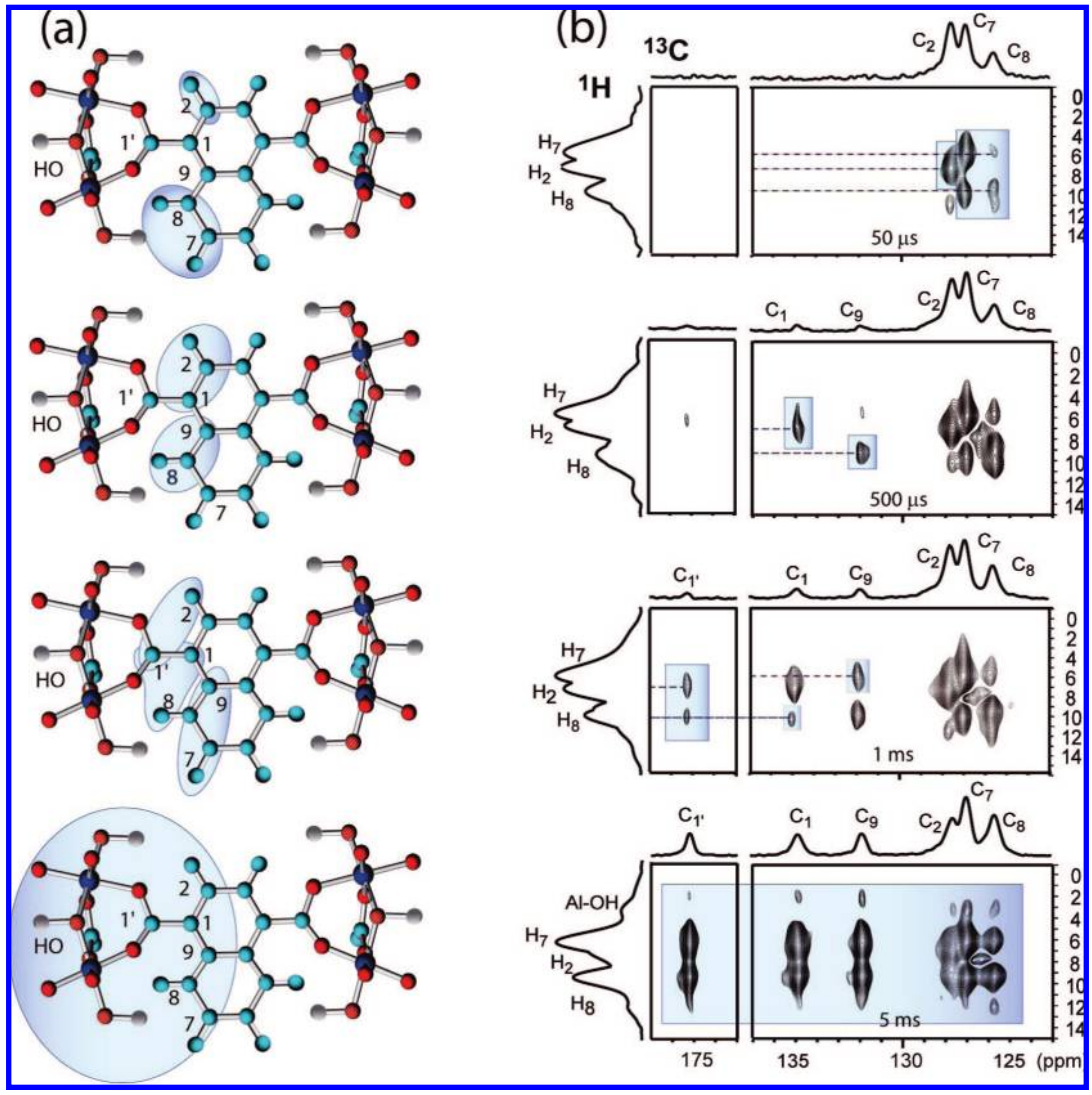

Figure 3. (a) Structural motif of the nanoporous Al(OH)(1,4-NDC) compound showing the Al–OH–Al chains interconnected by the 1,4-naphthalenedicarboxylate groups. The hydrogens of OH groups are modeled according to the geometry of the Al–OH–Al chains. The areas, highlighted blue, show the interaction sphere of hydrogens with the neighboring carbons at mixing times of 50 s, 500 s, 1 ms, and 5 ms of 2D NMR experiments. (b) 2D ^{1}H−^{13}C Lee-Goldburg heterocorrelated NMR spectra of the nanoporous compound at different mixing times.

nuclei of the framework. At a contact time as short as 50 μs, the correlations between hydrogens and their covalently bonded carbons are apparent. Due to the remarkable resolution achieved by the Lee-Goldburg decoupling, the three aromatic hydrogens can be singly detected at δ_H = 6.1, 7.0, and 9.4 ppm and assigned to H_7, H_2, and H_8, respectively. At increasing contact times, the interaction sphere of hydrogens with neighboring carbons expands and through-space correlations involve carbons at larger distances as shown in Figure 3a. At contact times of 500 μs, also carbons that are not directly bonded to hydrogens and sit at distances shorter than 2.3 Å´ are included in the correlation pattern. Thus, the nonbonded correlations between H_2--C_1 and H_8--C_9 within the naphthalene building blocks are observed. Carboxylic carbons receive the magnetization from the aromatic hydrogens only at contact times longer than 1 ms, namely, from hydrogens H_2 and H_8 placed at a distance of 2.5−2.7 Å. No correlations are detected between H_7 hydrogens and carboxylic groups, being located at longer distances. At 5 ms contact times, the correlations involve the upfield signals in the hydrogen domain attributed to the OH groups sitting on the oxygens of the inorganic Al−O−Al chains. The 2D NMR spectra can demonstrate that the OH groups are in close relationship with the organic moieties. In fact, the hydrogen signal, resonating at 2.2 ppm, correlates with the non protonated carbons $C_{1'}$, C_1, and C_9 of the organic moieties. A further proton signal at 3.2 ppm is due to the presence of residual water molecules under exchange with OH groups (Supporting Information). This signal correlates with the protonated aromatic carbons C_2, C_7, and C_8, demonstrating that the OH/H_2O hydrogens and the CH aromatic groups belong to the same spin-system and to a restricted region of the space. The NMR results confirm the formation of a highly symmetric crystal structure that presents parallel and independent nanochannels of both large and small cross-sections.

HP ^{129}Xe NMR is a method of choice to understand the nature of the pore walls and the space available to the diffusing gases. This technique is specifically sensitive to the void spaces and complementary to conventional techniques that describe the solid part of the material. In addition, it is a noninvasive technique and does not affect the crystal structure. Thus, xenon is a direct and unique probe of channel structure and mimics the behavior of guest atoms or molecules that are confined to the restricted

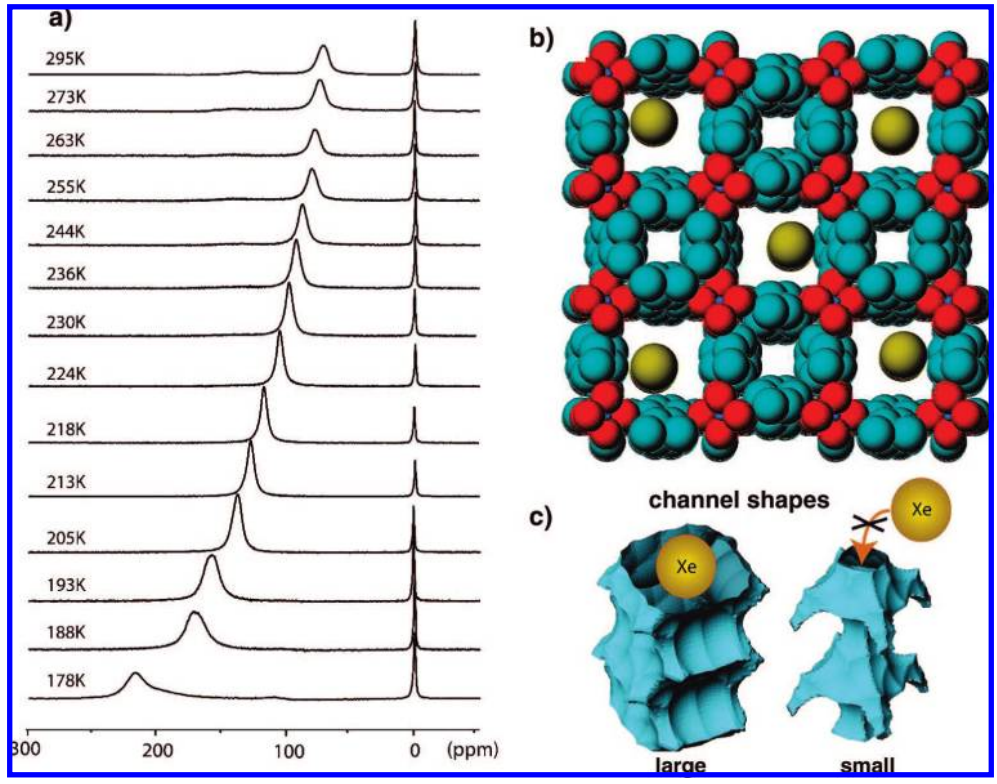

Figure 4. (a) Continuous-flow hyperpolarized ^{129}Xe NMR spectra of sample **2** at variable temperatures: the peak at 0 ppm is due to the free xenon and the downfield peak to the xenon exploring the nanochannels. (b) Crystal structure of sample **2**, viewed along the channel axis. The large channels are partially occupied by xenon atoms at low pressure. (c) Representation of the shape of large (7.7 × 7.7 Å^2) and small (3.0 × 3.0 Å^2) nanochannels as described by a center of a sphere of 0.6 Å radius rolling over their walls. Xenon atoms (4.4 Å diameter) can diffuse in the large channels but cannot enter in the small channels. Colors are as follows: carbon, light blue; oxygen, red; aluminum, blue; xenon, yellow.

space available. The hyperpolarized technique was applied to the sample endowed with channel-like structure and permanent porosity. HP ^{129}Xe NMR experiments, in the continuous flow mode, enabled the detection of xenon diffused to the nanochannels, in addition to the gas signal at 0 ppm (Figure 4). The hyperpolarized ^{129}Xe NMR spectrum of the nanoporous compound, performed at 295 K, reveals a narrow and symmetric signal at $\delta_{Xe} = 71.8$ ppm. The downfield signal is diagnostic of xenon exploring the nanochannels, and the absence of an anisotropic line shape shows that the channels are not narrow enough to impose their anisotropy to the xenon signal.[19] From theoretical and experimental studies of ^{129}Xe NMR on zeolites, we can deduce that a chemical shift value of 72 ppm, under the extreme dilution limit, corresponds to a pore size of about 9 Å, which is consistent with the channels of 7.7 × 7.7 Å^2 cross-section and a diagonal size of 10.5 Å. Thus, ^{129}Xe NMR provides a direct measurement of the void space and demonstrates unequivocally that the large channels are completely free from any guests and, in particular, from water. The xenon resonance could be collected at a concentration as low as 2% (see Experimental Section), that at room temperature allows the exclusive observation of xenon-wall interactions, xenon−xenon interactions being virtually absent. Lowering the temperature, there is a downfield shift due to the increased residence time of xenon on the internal surfaces. This behavior is opposite to the observed trend for a xenon in narrow-pipes and similar to the middle-size pore zeolites as NaY,[20] describing a rare example of zeolite-like material containing permanent and open channels large enough to accommodate more than one xenon per cross-section. At temperatures below 205 K, the increase in line width is due to a massive xenon condensation in the channels and the dramatic downfield shift at lower temperatures to the condensation on the external surfaces of the particles. The narrowing of the peak at higher temperature indicates the homogeneous void space explored by xenon. These results demonstrate that the large channels are open and available to be explored by the xenon gas atoms. Indeed, any occlusions or bottlenecks in the framework due to localized collapse of the crystalline structure would hinder effective communication between the cavities and the gas phase. Thus, the proposed method provides unique evidence for the absence of structural defects along the channels in the crystals. Moreover, at room temperature also a low intensity signal at 130 ppm is detectable in the spectrum, and this is likely due to a minor amount of xenon exploring the small channels. Therefore, small channels with 3.0 × 3.0 Å^2 cross-section are hardly accessible. The nanoporous compound has also been heated in situ up to 150 °C, but no substantial diffusion of xenon into the small channels has been observed since the limited cross-section of the 3.0 × 3.0 Å^2 is considerably smaller than the Xe van der Waals diameter of 4.4 Å. Thus,

(19) (a) Jameson, C. J.; de Dios, A. C. *J. Phys. Chem.* **2002**, *116*, 3805–3821. (b) Sozzani, P.; Comotti, A.; Simonutti, R.; Meersman, T. L.; Pines, A. *Angew. Chem., Int. Ed.* **2000**, *39*, 2695–2698. (c) Comotti, A.; Bracco, S.; Ferretti, L.; Mauri, M.; Simonutti, R.; Sozzani, P. *Chem. Commun.* **2007**, 350–352. (d) Moudrakosvki, I. L.; Soldatov, D. V.; Ripmeester, J. A.; Sears, D. N.; Jameson, C. J. *Proc. Natl. Acad. Sci. U.S.A.* **2004**, *101*, 17924. (e) Ueda, T.; Eguchi, T.; Nakamura, N.; Wasylishen, R. E. *J. Phys. Chem. B* **2003**, *107*, 180–185.

(20) (a) Jameson, C. J. *J. Am. Chem. Soc.* **2004**, *126*, 10450–10456. (b) Labouriau, A.; Pietrass, T.; Weber, W. A.; Gates, B. C.; Earl, W. L. *J. Phys. Chem. B* **1999**, *103*, 4323–4329.

at the low partial pressure of 0.02, a selective adsorption of xenon in the large channels occurs, showing that there exists a selective recognition of the two channels based on the size of the guests (Figure 4c); guests with two dimensions larger than 3.0 Å are selectively excluded by the smaller channels and are allowed to be adsorbed only by the larger channels. From the fitting of the chemical shift data as a function of temperature,[21] the enthalpy of adsorption of 10 kJ mol^{-1} has been evaluated. The enthalpy value falls in the range of physisorption phenomena and compares favorably the values reported for methane adsorption at low pressure in similar alumino organic compounds.[22] The value is twice that found in most molecular organic frameworks,[6f] suggesting that xenon is in close contact with a larger amount of surface in 1D nanochannels.

From the analysis of the two resonances belonging to the free gas and the xenon exploring the nanochannles at $\delta_s = 71.8$ ppm, the exchange dynamics of xenon between the confined space and the gas phase can be evaluated. In the hyperpolarized ^{129}Xe NMR spectrum at room temperature, the two signals resonate at 5460 Hz apart, indicating that the exchange time between the two states, if any exchange occurs, must be longer than 0.2 ms (the time τ can be determined in the fast exchange limit by the formula $\tau \cdot \Delta\omega \leq 1$, where $\Delta\omega$ is the difference of the xenon chemical shifts). However, a massive exchange must occur within 200 ms, as a $\pi/2$ pulse generates an intense signal of hyperpolarized xenon diffused in the porous material after 200 ms from the cancelation of the magnetization. To evaluate the exchange times on intermediate scales, the targeted experiment of hyperpolarized 2D^{129}Xe exchange NMR could be employed to achieve the goal.[23] The experiment was performed at room temperature, with mixing times ranging from 1 to 50 ms (Figure 5).

At 1 ms of exchange time virtually no cross-peaks are present, but starting from a mixing time of 15 ms cross-peaks appear and their intensity increases constantly with the increasing of mixing times. Figure 5b shows the traces at 0 ppm of the spectra, highlighting the comparison of the cross-peak and the diagonal peak intensities. The 2D experiments straightforwardly demonstrate that the nanopores are open and easily accessible by the gas phase within times as short as a few milliseconds. Thus, the crystals do not present irregularities on the surface or pore-obstructions at the channel ends that would prevent the access to the inner part of the crystals from their surfaces. The open channel structure, also open on the surface of the crystals, is crucial for the absorption properties of the material. In continuous flow conditions we can observe separately the exchange peaks of xenon exploring first the free gas and then the confined space (diffusing-in) as well as xenon diffusing-out.[24] In the present case, the intensities of both diffusing-in and -out cross-peaks are essentially balanced guaranteeing that the relaxation times are sufficiently long to allow the detection of the reversible pathway of xenon from the nanopores to the bulk gas.

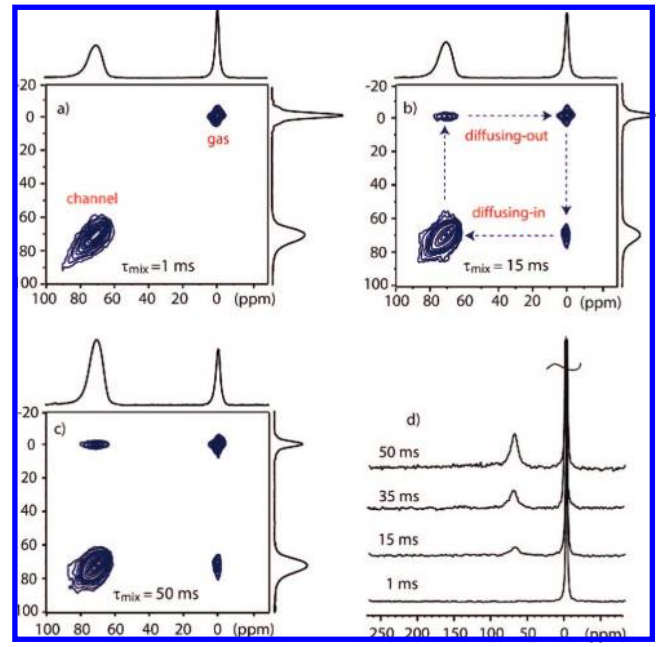

Figure 5. Continuous flow hyperpolarized 2D exchange hyperpolarized ^{129}Xe NMR experiments of sample **2** acquired at mixing times τ_m of (a) 1 ms, (b) 15 ms, and (c) 50 ms. (d) ^{129}Xe NMR traces of the 2D exchange spectra at 0 ppm.

Vapor and Gas Adsorption. To elucidate the permanent porosity and the nature of pores of compound **2**, adsorption isotherms of various guests were performed. The adsorption isotherm of N_2 at 77 K shows that only surface adsorption occurs, indicating that N_2 molecules do not diffuse to the channels at low temperature even if the pore diameter is suitable for N_2 to pass through the large nanochannels (Figure 6a). This behavior has already been described in MOFs with pore sizes of less than 10 Å.[25] The CO_2 (surface area = 17.9 $Å^2$, kinetic diameter = 3.3 Å) adsorption isotherm at 195 K is described by a type-I curve[26] demonstrating the microporosity of the framework in agreement with the HP ^{129}Xe NMR results. The saturation capacity of CO_2 is up to 138 cm^3 (STP) g^{-1}, corresponding to 1.6 CO_2 moles per mole of naphthalene moiety. The volume occupied by stored CO_2 corresponds to 443 $Å^3$ per unit cell and is consistent with the empty volume of the large nanochannel as can be estimated by the crystal structure. The surface area accessible to carbon dioxide, evaluated as 546 m^2 g^{-1} by the Langmuir equation, corresponds to the theoretical surface area of 532 m^2 g^{-1} calculated for the large channels.[27] The quadrupole moment of carbon dioxide molecule explains the remarkable uptake since it can promote favorable interactions with the host due to the presence of polar groups and π-electron clouds. A contribution for favorable CO_2 adsorption can be due to the presence of OH groups protruding toward the channels. These results are consistent with the inaccessibility of the small 3.0 × 3.0 $Å^2$ nanochannels to carbon

(21) Terskikh, V. V.; Mudrakovskii, I. L.; Mastikhin, V. M. *J. Chem. Soc., Faraday Trans.* **1993**, *89*, 4239–4243.
(22) Loiseau, T.; Lecroq, L.; Volkringer, C.; Marrot, J.; Férey, G.; Haouas, M.; Taulelle, F.; Bourrelly, S.; Llewellyn, P. L.; Latroche, M. *J. Am. Chem. Soc.* **2006**, *128*, 10223–10230.
(23) (a) Knagge, K.; Smith, J. R.; Smith, L. J.; Buriak, J.; Raftery, D. *Solid State Nucl. Magn. Reson.* **2006**, *29*, 85–89. (b) Tallavaara, P.; Jokisaari, J. *Phys. Chem. Chem. Phys.* **2006**, *8*, 4902–4907.
(24) (a) Anala, S.; Pavlovskaya, G. E.; Pichumani, P.; Dieken, T. J.; Olsen, M. D.; Meersmann, T. *J. Am. Chem. Soc.* **2003**, *125*, 13298–13302. (b) Cheng, C. Y.; Bowers, C. R. *J. Am. Chem. Soc.* **2007**, *129*, 13997–14002. (c) Simonutti, R.; Bracco, S.; Comotti, A.; Mauri, M.; Sozzani, P. *Chem. Mater.* **2006**, *18*, 4651–4657.
(25) (a) Chen, B. L.; Ma, S. Q.; Zapata, F.; Fronczek, F. R.; Lobkovsky, E. B.; Zhou, H. C. *Inorg. Chem.* **2007**, *46*, 1233–1236. (b) Vaidhyanathan, R.; Bradshaw, D.; Rebilly, J. N.; Barrio, J. P.; Gould, J. A.; Berry, N. G.; Rosseinsky, M. J. *Angew. Chem., Int. Ed.* **2006**, *45*, 6495–6499. (c) Maji, T. K.; Matsuda, R.; Kitagawa, S. *Nat. Mater.* **2007**, *6*, 142–148.
(26) Sing, K. S. W.; Everett, D. H.; Haul, R. A. W.; Moscou, L.; Pierotti, R. A.; Rouquerol, J.; Siemieniewska, T. *Pure Appl. Chem.* **1985**, *57*, 603–619.
(27) The surface area (m^2 g^{-1}) has been calculated by a simplified method that takes into account two large channels with square cross-sections of 7.7 × 7.7 $Å^2$ per unit cell with respect to the mass of the matter.

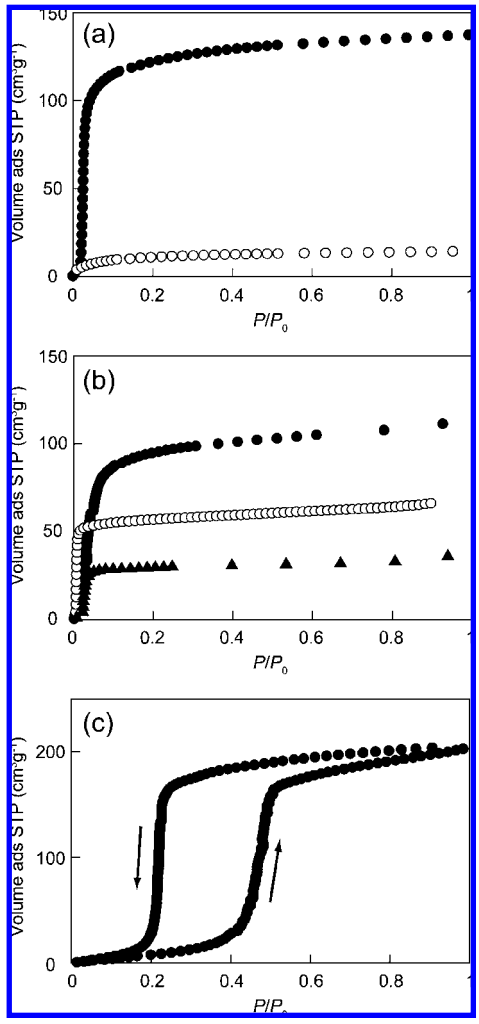

Figure 6. Adsorption isotherms of **2** for (a) CO_2 (●, 195 K) and N_2 (○, 77 K), (b) methanol (●), acetone (○), benzene (▲) at 298 K, and adsorption/desorption isotherms of (c) H_2O at 298 K.

dioxide, likely due to the steric exclusion, and agreed with the selective adsorption of xenon as shown by Xe NMR spectroscopy. Vapors, such as methanol and acetone, are also adsorbed efficiently showing Langmuir type-I curves (Figure 6b). The saturation capacity for methanol and acetone are 112 and 66 cm^3 (STP) g^{-1}, respectively, indicating that 5 and 2.9 molecules per unit cell are stored. Taking into account the volumes of the molecules of 67.2 and 122 $Å^3$ for methanol and acetone, respectively,[28] we calculate an occupied value of 340 $Å^3$ per unit cell, which is close to the full loading of the large channels indicating that the guest stabilization is remarkable and the nanochannel capacity is the limiting factor. In the case of benzene the lower loading of 1.1 molecules per unit cell at $P/P_0 = 0.95$, which corresponds to an occupied volume of 37% with respect to that of CO_2, suggests a looser interaction of the apolar benzene molecules with the framework.

Interestingly, the adsorption isotherm of water shows no uptake up to 9.5 mmHg (Figure 6c) followed by a steep rise and the attainment of the saturation capacity of 204 cm^3 g^{-1} (8.9 molecules per unit cell) at $P/P_0 = 0.4$ with a large hysteresis loop; thus, it can be classified as type V. The existence of a pressure threshold is less common in PCPs since most PCPs show a high affinity for the presence of hydrophilic sites in their frameworks. The behavior of Al(OH)(1,4-NDC) is instead typical of hydrophobic pore surfaces,[29] and this behavior suggests the formation of only weak guest−wall interactions as a consequence of the presence of naphthalene rings lining the nanochannel walls. This hydrophobic behavior has been previously described in the literature for microporous materials such as aluminosilicate-based zeolites and activated carbons.[30] The selective adsorption of methanol and acetone with respect to water, that occurs at low partial pressure, is intriguing for the potentiality of the host toward vapor separation. The adsorption results confirm the formation of a permanently porous PCP compound that presents not only the channel opening, as in conventional zeolites, but also organic groups that focus specific interactions on the channel core and fabricate metal−organic structures that cooperatively stabilize guests that diffuse in.

Conclusions

A novel porous coordination polymer was studied by means of nonconventional diffractometric and spectroscopic techniques to understand the structure of both the framework and the cavities. For the first time, $^1H-^{13}C$ 2D Lee-Goldburg NMR spectra, exploiting through-space dipole−dipole heteronuclear interactions, were applied to PCPs to collect spatial relationships within the framework. In particular, hydroxyl groups and water molecules, which are hardly detectable by powder X-ray diffraction, have been located. The structure shows parallel and independent nanochannels of two different cross-sections that, depending on their size, can be selectively explored by gaseous species. Indeed, carbon dioxide is exclusively adsorbed into the large channels, leaving the small channels available, with the intriguing perspective of selective adsorption of small gases such as hydrogen. The unconventional technique of hyperpolarized xenon NMR could show, with extremely high sensitivity, the easy accessibility of the large channels to xenon and determine the average 9 Å cross-section of the channels. In particular, it is shown that virtually no restrictions or relevant amount of defects are present in the structure such as to prevent diffusion from the gas phase to the open large nanochannels, while small nanochannels are inaccessible to xenon because of geometrical constraints. By exploring the cavities, we could detect the signal of included xenon after a few milliseconds of diffusion in the material, collecting information about the channel geometry, the adsorption energy and exchange phenomena. The absence of multiple peaks in the ^{129}Xe NMR spectra in the temperature range from 178 to 295 °C reflects the homogeneous surface structure of the PCP compound in excellent agreement with the geometry of the nanochannels proposed by powder X-ray synchrotron diffraction data. 2D exchange Xe NMR enabled the establishment of the time for exchange dynamics of xenon between the bulk gas phase and the confined space in the coordinative architecture. This evidence opened up the way to explore the adsorption properties of important gases such as carbon dioxide and the selective adsorption of vapors, such as methanol and acetone vs water, by exploiting the weak intermolecular interactions between host and guests.

(28) The densities in the liquid phase, for both methanol and acetone, are 0.79 g cm^{-3}.

(29) (a) Horike, S.; Tanaka, D.; Nakagawa, K.; Kitagawa, S. *Chem. Commun.* **2007**, 3395–3397. (b) Inagaki, S.; Fukushima, Y.; Kuroda, K.; Kuroda, K. *J. Colloid Interface Sci.* **1996**, *180*, 623–624.

(30) (a) Mahle, J. L. *Carbon* **2002**, *40*, 2753–2759. (b) McCallum, C. L.; Bandosz, T. J.; McGrother, S. C.; Muller, E. A.; Gubbins, K. E. *Langmuir* **1999**, *15*, 533–544. (c) Mahle, J. L. *Carbon* **2002**, *40*, 2753–2759.

This strategy, borrowed by supramolecular chemistry, enables intriguing applications for selective separation and purification.

Acknowledgment. We thank Fondazione Cariplo, FIRB (Italy), Exploratory Research for Advanced Technology (ERATO), and Japan Science and Technology Agency (JST) for financial support. We are grateful to M. Mauri for support of NMR experiments.

Supporting Information Available: Crystal structure of the compound **1**, thermogravimetric analysis, ^{13}C relaxation times, ^{13}C CP, and ^{1}H MAS NMR spectra of compounds **1** and **2**. This material is available free of charge via the Internet at http://pubs.acs.org.

JA802589U